

Ratio of σ_L/σ_T for $p(e, e'K^+)\Lambda$ Extracted from Polarization Transfer

Brian A. Raue*

Florida International University, Miami, FL 33199

Daniel S. Carman†

Ohio University, Athens, OH 45701

(Dated: November 9, 2018)

Abstract

The ratio of longitudinal to transverse structure functions, σ_L/σ_T , has been extracted from recent beam-recoil transferred polarization data for the $p(\vec{e}, e'K^+)\vec{\Lambda}$ reaction. Results have been obtained for $W=1.72, 1.84,$ and 1.98 GeV at an average Q^2 of $0.77, 0.69,$ and 0.61 GeV², respectively. Our results indicate a ratio that is systematically slightly smaller than previously published results using a Rosenbluth separation.

PACS numbers: 13.40.-f, 13.60.Rj, 13.88.+e, 14.20.Jn, 14.40.Aq

*Electronic address: baraue@fiu.edu

†Electronic address: carman@ohio.edu

I. INTRODUCTION

Data taken in Hall B at Jefferson Laboratory have recently been published on polarization transfer in the reaction $p(\vec{e}, e'K^+)\vec{\Lambda}$ [1]. While these data have been used to shed light on the $s\bar{s}$ quark pair creation operator in the associated strangeness production reaction, they cannot yet provide direct constraints on the isobar models commonly employed to describe the reaction mechanism [2]. These phenomenological models (e.g.[3, 4]) rely on fitting the available data to provide constraints on the contributing intermediate-state resonant and non-resonant processes in the s , t , and u reaction channels. The models differ in the set of specific resonant states included, as well as in their treatment of hadronic form factors and the restoration of gauge invariance. However, due to the sparsity of data for this reaction and the large number of parameters in the models, the contributions to the intermediate state remain largely unconstrained and, therefore, are highly uncertain.

The new polarization transfer data are difficult to include in fitting the isobar model parameters. This is due to the fact that, by necessity, these data were averaged over a large range in momentum transfer Q^2 (0.3 to 1.5 GeV²) and a large range in the invariant energy W (~ 200 MeV bins). The data have also been averaged over all Φ , the angle between the electron scattering plane and the $K^+\Lambda$ hadronic reaction plane (Fig. 1). One could expect significant variations in the model parameters over such large kinematic ranges. This means that including these data, say at their central kinematic values, into a global refit of the parameters is improper. Therefore these data have been employed only as a cross check of the model parameters based on fits to other measured observables.

The transferred polarization data can, however, provide useful new direct constraints to the models when they are used to extract the ratio of longitudinal to transverse structure functions, $R_\sigma = \sigma_L/\sigma_T$. This ratio has been previously measured using a Rosenbluth separation [5, 6, 7]. The results presented here provide a means of extracting R_σ that is less prone to systematic uncertainties than the Rosenbluth method and give results that are systematically slightly smaller.

II. FORMALISM

Following the notation of Ref. [8], the most general form for the virtual photoabsorption cross section in the center-of-mass frame (c.m.) from an unpolarized target, allowing for both a polarized electron beam and recoil hyperon, is given by:

$$\begin{aligned} \frac{d\sigma_v}{d\Omega_K^*} = & \mathcal{K} \sum_{\beta=0, x', y', z'} \left(R_T^{\beta 0} + \epsilon_L R_L^{\beta 0} + c_+ ({}^c R_{LT}^{\beta 0} \cos \Phi + {}^s R_{LT}^{\beta 0} \sin \Phi) \right. \\ & + \epsilon ({}^c R_{TT}^{\beta 0} \cos 2\Phi + {}^s R_{TT}^{\beta 0} \sin 2\Phi) \\ & \left. + hc_- ({}^c R_{LT'}^{\beta 0} \cos \Phi + {}^s R_{LT'}^{\beta 0} \sin \Phi) + hc_0 R_{TT'}^{\beta 0} \right). \end{aligned} \quad (1)$$

The $R_i^{\beta\alpha}$ are the transverse, longitudinal, and interference response functions that relate to the underlying hadronic current and implicitly contain the Λ polarization. The sum over β includes contributions from the hyperon polarization with respect to the (x', y', z') axes. In this system, \hat{z}' is along the outgoing K^+ direction, \hat{y}' is normal to the hadronic reaction plane, and $\hat{x}' = \hat{y}' \times \hat{z}'$ (Fig. 1). The $\beta = 0$ terms account for the unpolarized response and $\alpha=0$ implies an unpolarized target. The response functions denoted by $R_{LT'}$ and $R_{TT'}$ depend on the electron beam helicity h . The left superscripts on the response functions, c or s , indicate whether the term multiplies a sine or cosine term, respectively.

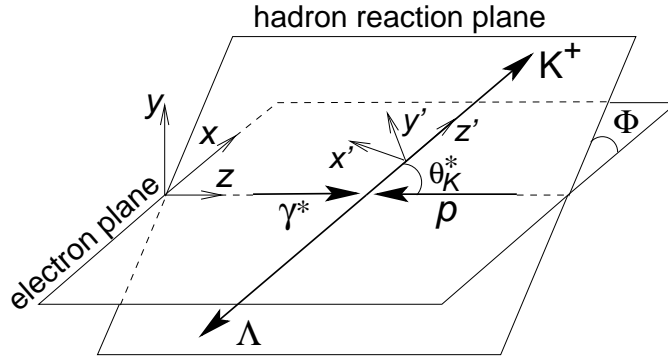


FIG. 1: Kinematics for $K^+\Lambda$ electroproduction showing angles and polarization axes in the center-of-mass reference frame.

The kinematic terms are defined by $c_{\pm} = \sqrt{2\epsilon_L(1 \pm \epsilon)}$ and $c_0 = \sqrt{1 - \epsilon^2}$, with the transverse and longitudinal polarization of the virtual photon defined respectively as $\epsilon = [1 + 2(1 + \nu^2/Q^2) \tan^2 \theta_e/2]^{-1}$ and $\epsilon_L = \epsilon Q^2/(k_{\gamma}^{c.m.})^2$. Here θ_e is the electron scattering angle, Q^2 is the negative of the four-momentum-transfer squared, ν is the virtual photon energy, and $k_{\gamma}^{c.m.}$ is the virtual-photon c.m. momentum. The leading factor $\mathcal{K} = |\vec{q}_K|/k_{\gamma}^{c.m.}$, where \vec{q}_K is the kaon c.m. momentum.

Using Eq.(1), the helicity-dependent hyperon polarization components, P' , in the (x', y', z') system are given by [1, 9]:

$$\begin{aligned}
\sigma_0 P'_{x'} &= \mathcal{K}(c_- {}^c R_{LT'}^{x'0} \cos \Phi + c_0 R_{TT'}^{x'0}), \\
\sigma_0 P'_{y'} &= \mathcal{K} c_- {}^s R_{LT'}^{y'0} \sin \Phi, \\
\sigma_0 P'_{z'} &= \mathcal{K}(c_- {}^c R_{LT'}^{z'0} \cos \Phi + c_0 R_{TT'}^{z'0}).
\end{aligned} \tag{2}$$

Here, σ_0 represents the unpolarized part of the cross section, which can be defined in terms of either response functions R_i or structure functions σ_i as:

$$\begin{aligned}
\sigma_0 &\equiv \frac{d\sigma_v}{d\Omega_K^*} = \mathcal{K} \left[R_T^{00} + \epsilon_L R_L^{00} + \sqrt{2\epsilon_L(1+\epsilon)} {}^c R_{LT}^{00} \cos \Phi + \epsilon {}^c R_{TT}^{00} \cos 2\Phi \right] \\
&= \sigma_T + \epsilon \sigma_L + \sqrt{2\epsilon(1+\epsilon)} \sigma_{LT} \cos \Phi + \epsilon \sigma_{TT} \cos 2\Phi,
\end{aligned} \tag{3}$$

where we note that $\sigma_T = \mathcal{K} R_T^{00}$ and $\epsilon \sigma_L = \mathcal{K} \epsilon_L R_L^{00}$.

The transferred polarization can also be defined in the (x, y, z) coordinate system where \hat{z} is along the virtual photon direction, \hat{y} is normal to the electron scattering plane, and $\hat{x} = \hat{y} \times \hat{z}$ (see Fig. 1). The components of P' in the (x, y, z) system are related to those in the (x', y', z') system by a simple rotation and are given by:

$$\begin{aligned}
P'_x &= P'_{x'} \cos \Phi \cos \theta_K^* - P'_{y'} \sin \Phi + P'_{z'} \cos \Phi \sin \theta_K^* \\
P'_y &= P'_{x'} \sin \Phi \cos \theta_K^* + P'_{y'} \cos \Phi + P'_{z'} \sin \Phi \sin \theta_K^* \\
P'_z &= -P'_{x'} \sin \theta_K^* + P'_{z'} \cos \theta_K^*,
\end{aligned} \tag{4}$$

where θ_K^* is the K^+ c.m. polar angle defined in Fig. 1.

If the transferred polarization components are now integrated over all Φ (calling these components \mathcal{P}'), Eq.(2) simplifies to:

$$\mathcal{P}'_{x'} = \frac{c_0 R_{TT'}^{x'0}}{R_T^{00} + \epsilon_L R_L^{00}}, \quad \mathcal{P}'_{z'} = \frac{c_0 R_{TT'}^{z'0}}{R_T^{00} + \epsilon_L R_L^{00}}, \tag{5}$$

and Eq.(4) simplifies to:

$$\begin{aligned}
\mathcal{P}'_x &= \frac{c_- ({}^c R_{LT'}^{x'0} \cos \theta_K^* - R_{LT'}^{y'0} + {}^s R_{LT'}^{z'0} \sin \theta_K^*)}{R_T^{00} + \epsilon_L R_L^{00}}, \\
\mathcal{P}'_z &= \frac{c_0 (-R_{TT'}^{x'0} \sin \theta_K^* + R_{TT'}^{z'0} \cos \theta_K^*)}{R_T^{00} + \epsilon_L R_L^{00}}.
\end{aligned} \tag{6}$$

The components of \mathcal{P}' along the \hat{y} and \hat{y}' axes are identically zero from the integration of Eqs.(2) and (4) over $0 \leq \Phi \leq 2\pi$. Such an integration was performed on the polarization

transfer data of Ref. [1] in which acceptance corrections were first applied to raw yields before summing over all Φ angles. This had the effect of improving statistical uncertainties on the measured transferred polarizations. It also provided a systematics check in that the \hat{y} and \hat{y}' components of the polarization were found to be zero to within statistical uncertainties.

Concentrating now on the z' and z components in parallel or anti-parallel kinematics ($\cos \theta_K^* = \pm 1$), Eqs.(5) and (6) reduce to:

$$\mathcal{P}'_{z'} = \pm \mathcal{P}'_z = \pm \frac{c_0 R_{TT'}^{z'0}}{R_T^{00} + \epsilon_L R_L^{00}} = \pm \frac{c_0 R_{TT'}^{z'0}}{\sigma_u / \mathcal{K}}, \quad (7)$$

where the plus (minus) sign is associated with the parallel (anti-parallel) kinematics case and $\sigma_u = \sigma_T + \epsilon \sigma_L$.

The response functions of Eqs.(5) and (6) can be written in terms of the CGLN amplitudes [10] as shown in Ref. [8] as:

$$R_{TT'}^{x'0} = \sin \theta_K^* \text{Re} \left[-|F_1|^2 + |F_2|^2 + F_2^* F_3 - F_1^* F_4 + \cos \theta_K^* (F_2^* F_4 - F_1^* F_3) \right], \quad (8)$$

$$R_{TT'}^{z'0} = \text{Re} \left[-2F_1^* F_2 + \cos \theta_K^* (|F_1|^2 + |F_2|^2) - \sin^2 \theta_K^* (F_1^* F_3 + F_2^* F_4) \right], \quad (9)$$

$$R_T^{00} = |F_1|^2 + |F_2|^2 + \frac{\sin^2 \theta_K^*}{2} (|F_3|^2 + |F_4|^2) + \text{Re} \left[\sin^2 \theta_K^* (F_2^* F_3 + F_1^* F_4 + \cos \theta_K^* F_3^* F_4) - 2 \cos \theta_K^* F_1^* F_2 \right], \quad (10)$$

$$R_L^{00} = \text{Re} \left[|F_5|^2 + |F_6|^2 + 2 \cos \theta_K^* F_5^* F_6 \right]. \quad (11)$$

For the case of $\theta_K^* = 0$, these forms simplify to:

$$R_{TT'}^{x'0} = 0, \quad R_{TT'}^{z'0} = R_T^{00} = |F_1 - F_2|^2, \quad \text{and} \quad R_L^{00} = |F_5 + F_6|^2. \quad (12)$$

Combining the result of Eq.(12) with Eq.(7) we obtain for $\theta_K^* = 0$:

$$\mathcal{P}'_{z'} = \mathcal{P}'_z = \frac{c_0 R_T^{00}}{R_T^{00} + \epsilon_L R_L^{00}}. \quad (13)$$

This expression can then be inverted to determine the ratio of the longitudinal to transverse response functions [9], or alternatively, the ratio of $R_\sigma = \sigma_L / \sigma_T$ as:

$$R_\sigma = \frac{\sigma_L}{\sigma_T} = \frac{1}{\epsilon} \left(\frac{c_0}{\mathcal{P}'_{z'}} - 1 \right). \quad (14)$$

III. EXTRACTION OF R_σ

Figure 2 reproduces the results from Ref. [1] along with sample model calculations. The kinematic values and the most forward-angle data points are given in Table I. The values of $\langle W \rangle$ and $\langle Q^2 \rangle$ given in the table and the values of $\cos\theta_K^*$ shown in the figure are the average values over the kinematic bin and were determined by the distribution of the acceptance-corrected data within the bin. The curves correspond to the hydrodynamic models of Refs. [3] (solid) and [4] (dashed) and have been averaged over the kinematical bins. It is clear that the models badly miss in predicting polarization at nearly all values of $\cos\theta_K^*$ and, therefore, must fail to predict R_σ .

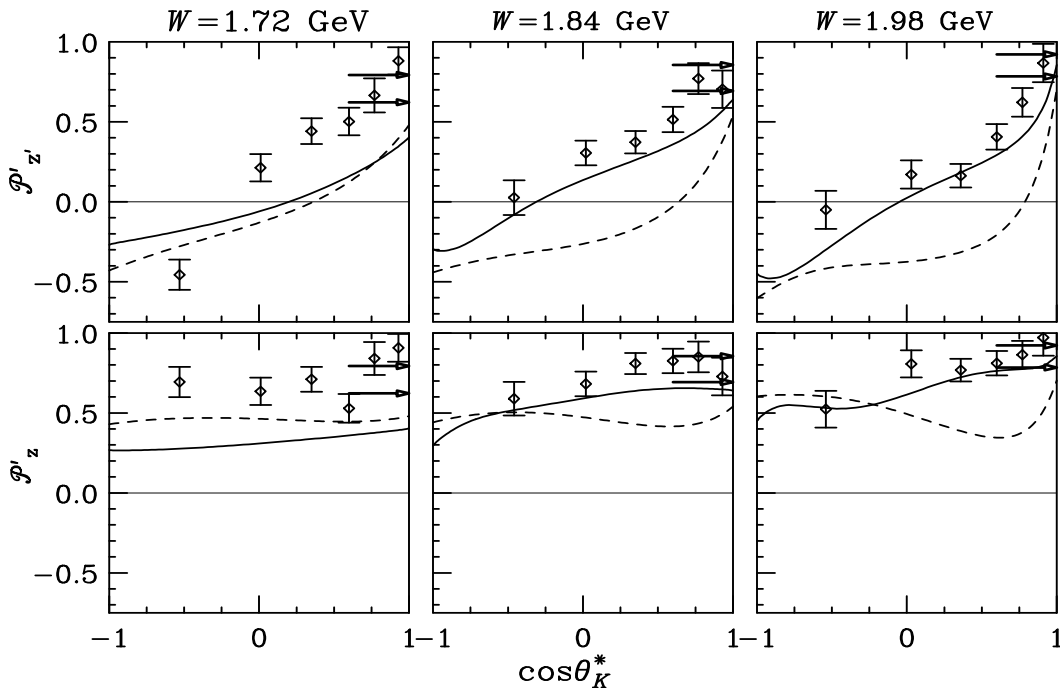


FIG. 2: Transferred Λ polarization projected along the z' (top) and z (bottom) axes versus $\cos\theta_K^*$ from Ref. [1]. The data were summed over Q^2 and Φ and are shown for three average values of W as indicated. The solid and dashed curves correspond to the hydrodynamic models of Refs. [3] and [4], respectively. The upper arrow in each plot indicates the maximum physically allowable value of the polarization at $\cos\theta_K^* = 1$, while the lower arrows indicate the polarization corresponding to $R_\sigma = 0.45$.

Since both R_L^{00} and R_T^{00} must be positive definite, the ratio $R_\sigma \geq 0$. Thus, Eq.(14) gives a maximum value of $\mathcal{P}'_{z'} = \mathcal{P}'_z = c_0$ at $\cos\theta_K^* = 1$. This limiting value is shown by the upper arrow in each plot of Fig. 2. This arises from the fact that these response functions can be

written in terms of absolute squares of helicity amplitudes, as shown in Ref. [8], and must therefore always be greater than zero.

$\langle W \rangle$ GeV	$\langle Q^2 \rangle$ GeV ²	$\langle \epsilon \rangle$	$\mathcal{P}'_{z'} \pm \Delta\mathcal{P}'_{z'}$	$\mathcal{P}'_z \pm \Delta\mathcal{P}'_z$	$\mathcal{P}'_{z'}(x = 1)$
1.72	0.77	0.619	0.881±0.086	0.907±0.087	0.62
1.84	0.69	0.518	0.704±0.116	0.728±0.118	0.69
1.98	0.61	0.388	0.868±0.120	0.971±0.114	0.78

TABLE I: Transferred polarization data at $\cos\theta_K^* = 0.93$ from Ref. [1] at the average kinematic quantities shown. The Q^2 range extends from 0.35 up to 1.4, 1.2, and 1.0 GeV² for the kinematic bins, respectively. The W ranges are 1.60 to 1.78 GeV, 1.78 to 1.90 GeV, and 1.90 to 2.15 GeV. The last column gives the values of $\mathcal{P}'_{z'}$ and \mathcal{P}'_z at $x \equiv \cos\theta_K^* = 1$ for a ratio of $R_\sigma = 0.45$ —the average value from Ref. [7].

The small-angle data of Ref. [1] cover an angular bin of $0.8 \leq \cos\theta_K^* \leq 1$ and therefore do not give direct access to $\mathcal{P}'_{z'}$ or \mathcal{P}'_z at $\cos\theta_K^* = 1$. However, the values of the polarization in the smallest angle bins and the trends of the data suggest some small difference from what is expected given the recent R_σ results of Mohring *et al.* [7]. The three Mohring data points at $Q^2=0.52, 0.75,$ and 1.00 GeV² and $W=1.84$ GeV give an approximate average value of $R_\sigma = 0.45$. This would give polarizations at $\cos\theta_K^* = 1$ shown by the lower arrows in the plots of Fig. 2 and also given in the last column of Table I. The Mohring results suggest a somewhat lower value for the polarization at $\cos\theta_K^* = 1$ than the trends of the polarization data at both $W = 1.72$ and 1.98 GeV indicate. One should probably not be too surprised by the apparent discrepancy between the polarization results at $W = 1.72$ GeV and the polarization value suggested by the Mohring data. This bin covers the threshold region where the $S_{11}(1650)$, $P_{11}(1710)$, and $P_{13}(1720)$ resonances are expected to play a significant role in $K\Lambda$ electroproduction [3, 4]. These resonances do not overlap significantly with the data of Mohring.

While the qualitative discussion above is useful in setting the stage, a reliable extrapolation of the \mathcal{P}' polarization data to $\cos\theta_K^* = 1$ is needed to determine R_σ . By combining the z' and z components of Eqs.(5) and (6) and rearranging, we get:

$$R_{sum} \equiv \frac{(\mathcal{P}'_{z'} + \mathcal{P}'_z)\sigma_u}{c_0} = \mathcal{K}[(1 + \cos\theta_K^*)R_{TT'}^{z'0} - R_{TT'}^{z0} \sin\theta_K^*]. \quad (15)$$

In this form, both Eqs.(7) and (14) will provide constraints on R_{sum} at $x \equiv \cos \theta_K^* = \pm 1$. At $x = -1$, the sum of the polarizations must be zero, according to Eq.(7), leading to $R_{sum}(x = -1) = 0$. This is an important useful constraint that can most easily be imposed on an extrapolation by using Eq.(15). Again using the fact that $R_\sigma \geq 0$, Eq.(14) leads to $R_{sum} \leq 2\sigma_u$ for $x = 1$. We will discuss the imposition of these constraints on the extrapolation shortly.

Besides the explicit θ_K^* dependence shown in Eq.(15) and in the response functions of Eqs.(8-11), the CGLN amplitudes contain additional θ_K^* dependence (as well as Q^2 and W dependence). This suggests that Eq.(15) can then be fit with polynomials in $x = \cos \theta_K^*$ provided we have prior knowledge of the σ_u term.

We have used the unpublished $p(e, e'K^+)\Lambda$ cross section data from CLAS of Feuerbach [12] to determine σ_u . In that work, the polarization-independent cross sections of Eq.(3) were measured over the complete angular range of $\cos \theta_K^*$ and Φ , and for similar values of W and Q^2 as in Ref. [1]. A simultaneous fit to the $\cos \theta_K^*$ and Φ dependence thus enabled the extraction of the $\cos \theta_K^*$ -dependent structure functions of Eq.(3): σ_u , σ_{LT} , and σ_{TT} . The cross section data were fit (8 Φ bins and 6 $\cos \theta_K^*$ bins per W and Q^2 bin) with a third-order polynomial in x . The resulting fit values were then combined with the polarization to calculate the corresponding values for R_{sum} at the kinematics for each of the data points in Fig. 2.

The number of terms one would include in a polynomial fit to Eq.(15) is ultimately governed by the reaction dynamics. The explicit θ_K^* dependence alone (see Eqs.(8-9)) suggests at least a third-order polynomial. However, given the limited number of polarization data points, the number of terms in any fit leading to a meaningful extrapolation to $\cos \theta_K^* = 1$ must also be limited. We begin by considering third-order fits of the form:

$$R_{sum} = a_0 + a_1x + a_2x^2 + a_3x^3. \quad (16)$$

We have done a series of fits to the data points representing R_{sum} in which we varied the number of terms in the fits while imposing the above constraints. The fitting routine is a variation of the Levenberg-Marquardt method [13] of minimizing χ^2 . A penalty was imposed on the χ^2 if a fit strayed too far from the constraints at $x = \pm 1$. Specifically, at $x = -1$, a penalty proportional to the deviation of $R_{sum}(x = -1)$ from zero was added to the χ^2 . To impose the constraint at $x = 1$, the χ^2 was multiplied by a penalty factor that was chosen

to be large enough to force non-negative values of R_σ . In determining the optimal number of parameters in the fit for each W bin, we simply used the number of parameters that produced the smallest minimized χ_ν^2 (χ^2 per degree of freedom).

We should point out that the $\mathcal{P}'_{z'}$ and \mathcal{P}'_z results of Ref. [1] were obtained from the same data set. Therefore, these observables are not independent. They do, however, measure different quantities (as seen by Eqs.(5) and (6)) since they are projections onto different axes. In adding these together to form R_{sum} , the uncertainties from $\mathcal{P}'_{z'}$ and \mathcal{P}'_z were added together.

For the two lowest W bins we found that a second-order polynomial in x was best for fitting R_{sum} and that a third-order polynomial was necessary for fitting the highest W bin. The fact that all W bins do not require the same order fit should not be surprising since the underlying physics (CGLN amplitudes) will contribute differently at different values of W . The results of our fits are shown in Fig. 3 (heavy solid lines) along with an error band (light solid lines). The error bands include uncertainties both from the fitting of Eq.(16), and also contributions from uncertainties in the fits of the cross section data. The latter contribution to the uncertainties is about half of that of the former. The error band indicates that the extrapolation to $x = 1$ is well constrained but that the back-angle fit is not. This is not surprising given the lack of data at back angles. However, the error bands do encompass the back-angle constraint that $R_{sum}(x = -1) = 0$. Table II shows the resulting χ_ν^2 and the polarization extrapolated to $x = 1$. The χ_ν^2 was determined after removing any penalties remaining in χ^2 .

We found that the resulting extrapolation of the polarization (and thus R_σ) at $x = 1$ is relatively insensitive to the exact form of the unpolarized cross section. We have done fits in which we varied the unpolarized cross section used in the fit by 10-20% (10% being the stated upper limit on systematic uncertainty of the unpolarized cross sections [12]) and observed negligible changes in the resulting value of R_σ . It is the polarization data that dominates the extrapolation and its associated uncertainties.

Plugging the extrapolated polarizations into Eq.(14) we can determine the ratio R_σ . These values are shown in the last column of Table II along with the combined uncertainties of the polarization and cross section fits and an estimated systematic uncertainty. Ref. [1] cites an absolute systematic error of less than 0.08 for each polarization point. Assuming a comparable systematic uncertainty for the extrapolated polarization at $x = 1$ leads to the

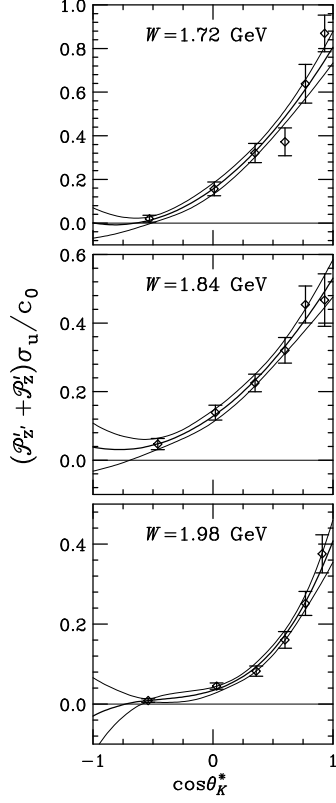


FIG. 3: R_{sum} (defined in Eq.(15)) versus $\cos\theta_K^*$ along with our fits (heavy solid lines) and the error band resulting from the fit and cross section uncertainties (light solid lines).

$\langle W \rangle$ GeV	$\langle Q^2 \rangle$ GeV ²	χ_ν^2	$\mathcal{P}'_{z',z}(x=1)$	R_σ
1.72	0.77	1.93	0.783 ± 0.072	$0.005 \pm 0.160 \pm 0.162$
1.84	0.69	0.35	0.782 ± 0.091	$0.239 \pm 0.252 \pm 0.232$
1.98	0.61	1.34	0.875 ± 0.080	$0.088 \pm 0.399 \pm 0.267$

TABLE II: Transferred polarization at $x = \cos\theta_K^* = 1.0$ extrapolated from the fits described in the text along with the resulting value of the ratio of transverse to longitudinal structure functions. Uncertainties on $\mathcal{P}'_{z',z}$ are the combined uncertainties arising from the fits to both the polarization and cross section data. The first uncertainty on R_σ is the statistical uncertainty (from the fit) while the second represents an estimated systematic uncertainty.

estimated systematic uncertainties on R_σ given in the table.

IV. DISCUSSION

The resulting values for R_σ are plotted in Fig. 4. For comparison, we have also included the previously published data [5, 6, 7]. We see that our results for R_σ using polarization transfer data are consistently smaller than the previous data obtained using the more common Rosenbluth separation method. In this method, the unpolarized cross section at a given Q^2 and W is measured in parallel kinematics as a function of ϵ . The cross section reduces to $\sigma_u = \sigma_T + \epsilon\sigma_L$. In principle, fitting the cross section data with a straight line gives σ_L and σ_T . However, this technique relies on a very precise determination of the absolute cross section at all ϵ points. To illustrate the inherent difficulties of this technique, one only needs to compare the results of Niculescu [6] with those of Mohring [7]. These are two analyses of the *same* data set taken in Hall C of Jefferson Lab. The Mohring results were published later and are generally believed to be more reliable. These data were measured at $W=1.84$ GeV—the same as our middle data point. Our own results are strikingly different than the Niculescu results and are slightly lower than—although within uncertainties of—the results of Mohring for points at comparable kinematics (lower two Q^2 points). We also observe that our highest Q^2 point is consistent with zero to within the extracted uncertainty. Again, comparison of this point to the results of Mohring is probably inappropriate because of the low average value of W for our point.

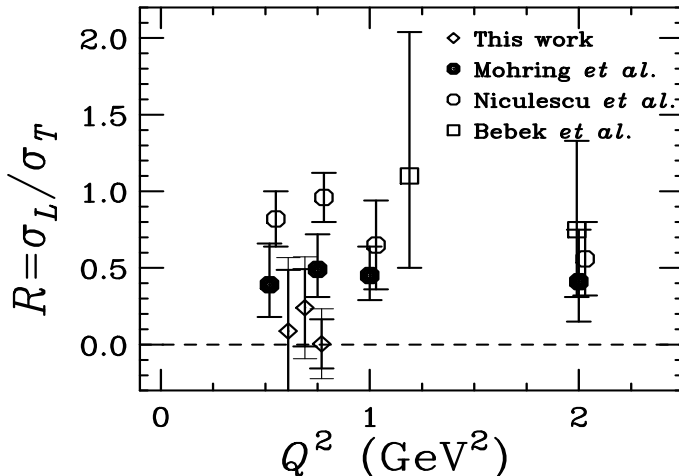


FIG. 4: Ratio of longitudinal to transverse structure functions vs. Q^2 . The inner error bars on our points represent the statistical uncertainties arising from the fit and the outer error bars represent the combination of statistical and estimated systematic uncertainties. The Niculescu results [6], which were superseded by the Mohring results [7], are offset in Q^2 for clarity.

Our result implies a small longitudinal structure function and hence a small longitudinal coupling of the virtual photon. In fact, at the highest Q^2 point (lowest W) our result is consistent with $\sigma_L = 0$. This structure function is expected to be very sensitive to the kaon form factor [15]. A recently conducted experiment in Hall A at Jefferson Laboratory [16] has as one of its main goals a Rosenbluth separation at several values of momentum transfer t leading to a Chew-Low extrapolation [17] of the kaon form factor. However, this method relies on having small *relative* uncertainties for σ_L . Therefore, if σ_L is as small as our results indicate, it seems unlikely that a reliable determination of the kaon form factor can be performed at these kinematics.

A more significant discrepancy between Rosenbluth and polarization-transfer results was previously observed in measurements of the ratio of the proton's electric and magnetic form factors, $\mu_p G_E/G_M$ (see Ref. [18] and references therein). The common wisdom is that the polarization-transfer method is much less susceptible to systematic errors. If one believes that the polarization transfer results are correct, then the slope derived from the Rosenbluth technique is too large. This is similar to what is implied by our results. One explanation that is being widely discussed is that there is an ϵ -dependent, two-photon-exchange effect that has not been properly accounted for in the radiative corrections applied to the experimental cross sections [19]. Some calculations [20] indicate that including this effect would bring down the high ϵ data points relative to the low ϵ data points and lead to better agreement between the Rosenbluth and polarization-transfer results. It is certainly premature to attribute the small differences between Rosenbluth results and our polarization-transfer results for $K^+\Lambda$ electroproduction to two-photon exchange. However, it is interesting that the trend of the differences is in the same direction as observed in the $\mu_p G_E/G_M$ results.

We would like to note that the polarization transfer data from which we extracted R_σ is just the first to come out of a larger program of kaon electroproduction in Hall B [21] at Jefferson Lab. Analysis is currently underway in which cross sections and polarization observables will be measured covering W from threshold up to 3.0 GeV and Q^2 from 0.3 up to 5 GeV². These data will yield a factor of 4 better statistical uncertainty for the Λ polarization transfer, thus leading to a more reliable determination of R_σ . Additional back-angle data will also allow extraction of R_σ in anti-parallel kinematics. In addition, Hall B will produce its own Rosenbluth separation that will complement both the existing data and results that are expected soon from Hall A [16]. We are eager to see if the apparent small

differences between the two techniques of extracting R_σ hold up with the coming results or are simply a case of statistical fluctuations.

In conclusion, we have done the first extraction of the ratio $R_\sigma = \sigma_L/\sigma_T$ from transferred polarization data for the $p(\vec{e}, e'K^+)\vec{\Lambda}$ reaction. Our results are systematically lower than the results obtained by the Rosenbluth technique and are also significantly different from model predictions. These results indicate a small longitudinal structure function for Q^2 of around 0.7 GeV^2 and W of 1.72, 1.84, and 1.98 GeV.

-
- [1] D.S. Carman *et al.*, Phys. Rev. Lett. **90**, 131804 (2003).
 - [2] C. Bennhold and S. Janssen, private communications.
 - [3] T. Mart and C. Bennhold, Phys. Rev. C **61**, 012201 (2000); H. Habermehl *et al.*, Phys. Rev. C **58**, R40 (1998).
 - [4] S. Janssen *et al.*, Phys. Rev. C **65**, 015201 (2002).
 - [5] C.J. Bebek *et al.*, Phys. Rev. D **15**, 3082 (1977).
 - [6] G. Niculescu *et al.*, Phys. Rev. Lett. **81**, 1805 (1998).
 - [7] R.M. Moring *et al.*, Phys. Rev. C **67**, 055205 (2003).
 - [8] G. Knöchlein, D. Dreschel, and L. Tiator, Z. Phys. A **352**, 327 (1995).
 - [9] H. Schmieden and L. Tiator, Eur. Phys. J. A **8**, 15 (2000).
 - [10] G.F. Chew *et al.*, Phys. Rev. **106**, 1345 (1957).
 - [11] H. Schmieden, Eur. Phys. J. A **1**, 427 (1998).
 - [12] Robert Feuerbach, Ph.D. Dissertation, Carnegie Mellon University, 2002.
 - [13] William H. Press, Brian P. Flannery, Saul A. Teukolsky, and William T. Vetterling, *Numerical Recipes: The Art of Scientific Computing* (Cambridge University Press, Cambridge, 1986).
 - [14] Philip R. Bevington and D. Keith Robinson, *Data Reduction and Error Analysis for the Physical Sciences, 2nd Ed.* (McGraw-Hill, Inc, 1992).
 - [15] B. Saghai, Nucl. Phys. **A639**, 217 (1998).
 - [16] P. Markowitz *et al.*, Jefferson Lab experiment E94-108.
 - [17] William R. Frazer, Phys. Rev **115**, 1763 (1959).
 - [18] J. Arrington, Phys. Rev. C **68**, 034325 (2003).
 - [19] J. Arrington, Phys. Rev. C **69**, 032201 (2004).

- [20] P.G. Blunden, W. Melnitchouk, and J.A. Tjon, Phys. Rev. Lett. **91**, 142304 (2003).
- [21] D.S. Carman *et al.*, Jefferson Lab experiments E99-006 and E00-112; K.H. Hicks *et al.*, Jefferson Lab experiment E93-030.